New hydrogen-rich ammonium metal borohydrides, $NH_4[M(BH_4)_4]$, M = Y, Sc, Al, as potential H_2 sources

A. Starobrat,[a,b] T. Jaroń[b*] and W.Grochala[b]

[a] College of Inter-Faculty Individual Studies in Mathematics and Natural Sciences (MISMaP), University of Warsaw, Banacha 2c, 02-097 Warsaw, Poland

[b] Centre of New Technologies, University of Warsaw, Banacha 2c, 02-097 Warsaw, Poland.

Contents

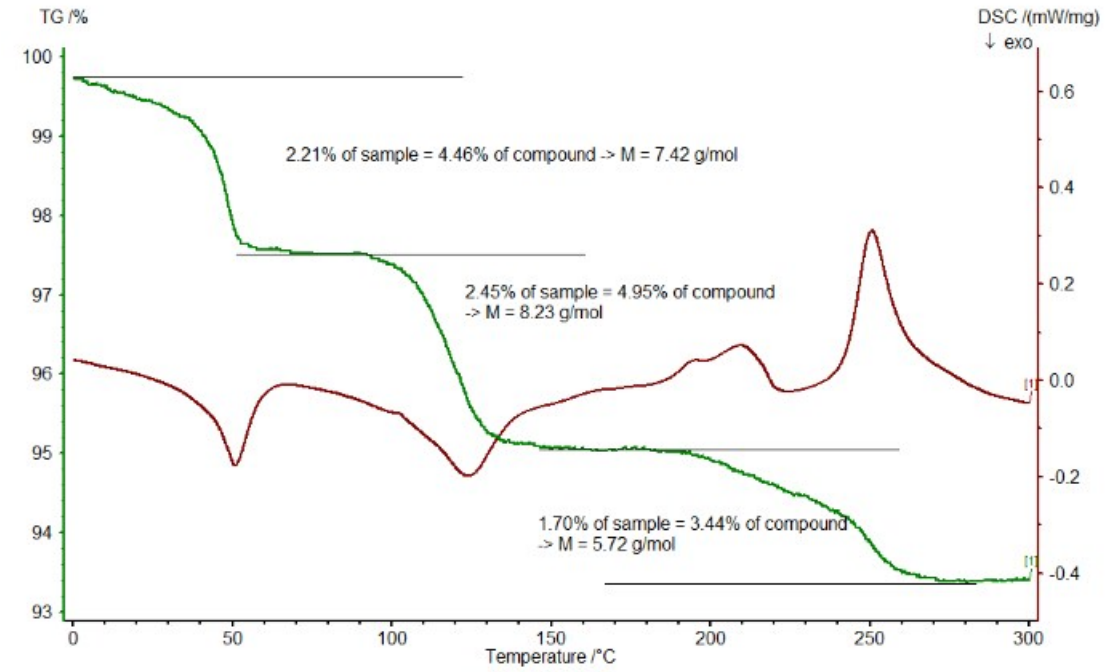

Figure S1. TGA/DSC plots of $NH_4[Y(BH_4)_4]$ (**1**) with quantitative details on mass drop events.

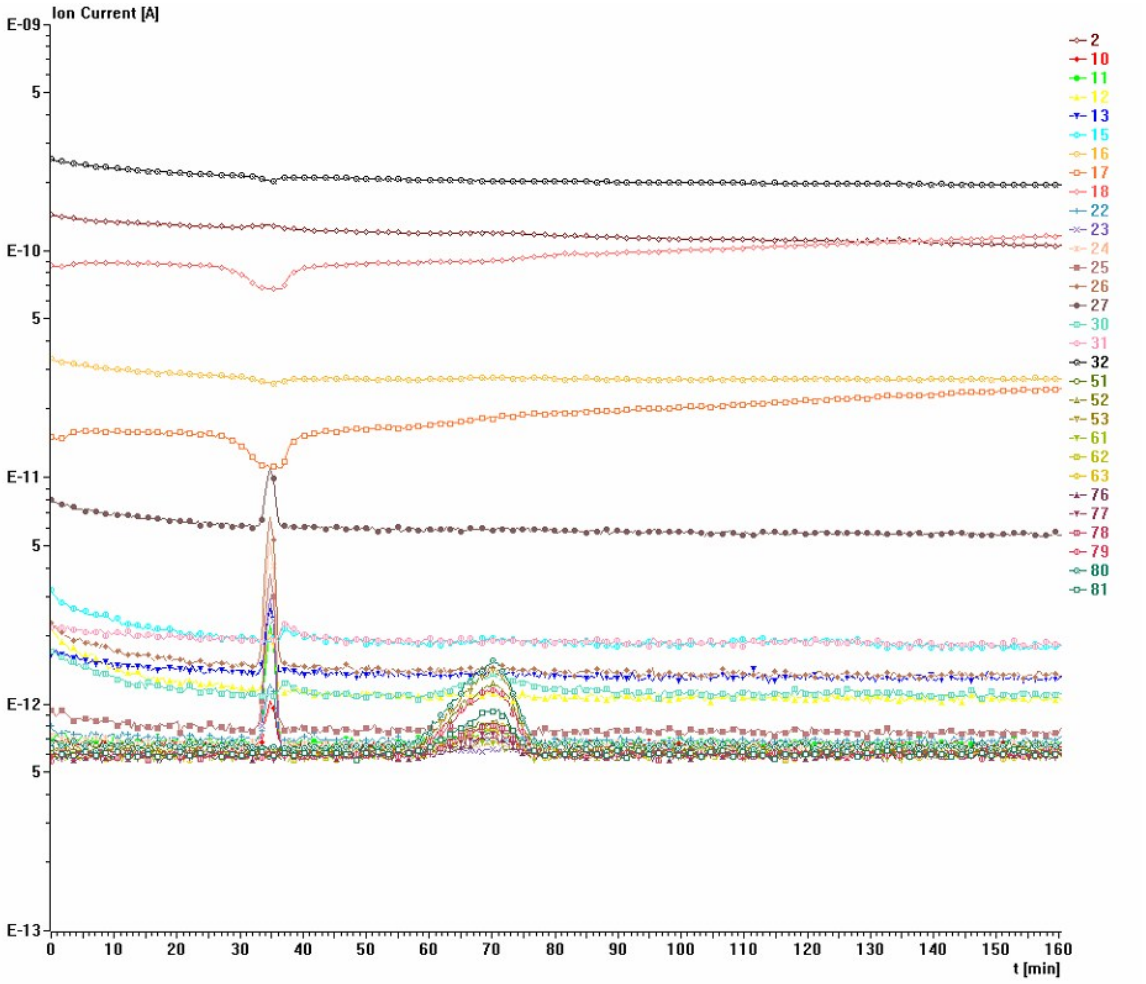

Figure S2. Mass spectra of gaseous decomposition products of compound **1**. Time range shown in the figure corresponds to temperature range -20–300 °C, heating rate 2 °C/min. Maxima of two main events can be observed at times corresponding to 50 °C and 120 °C.

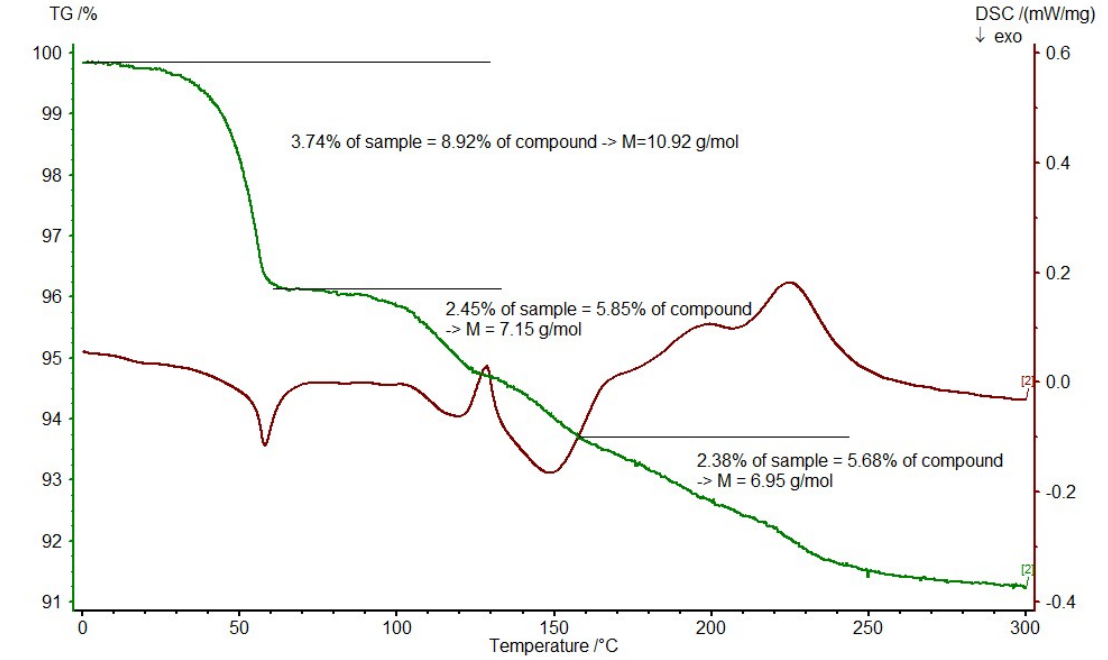

Figure S3. TGA/DSC plots of $NH_4[Sc(BH_4)_4]$ (**2**) with quantitative details on mass drop events.

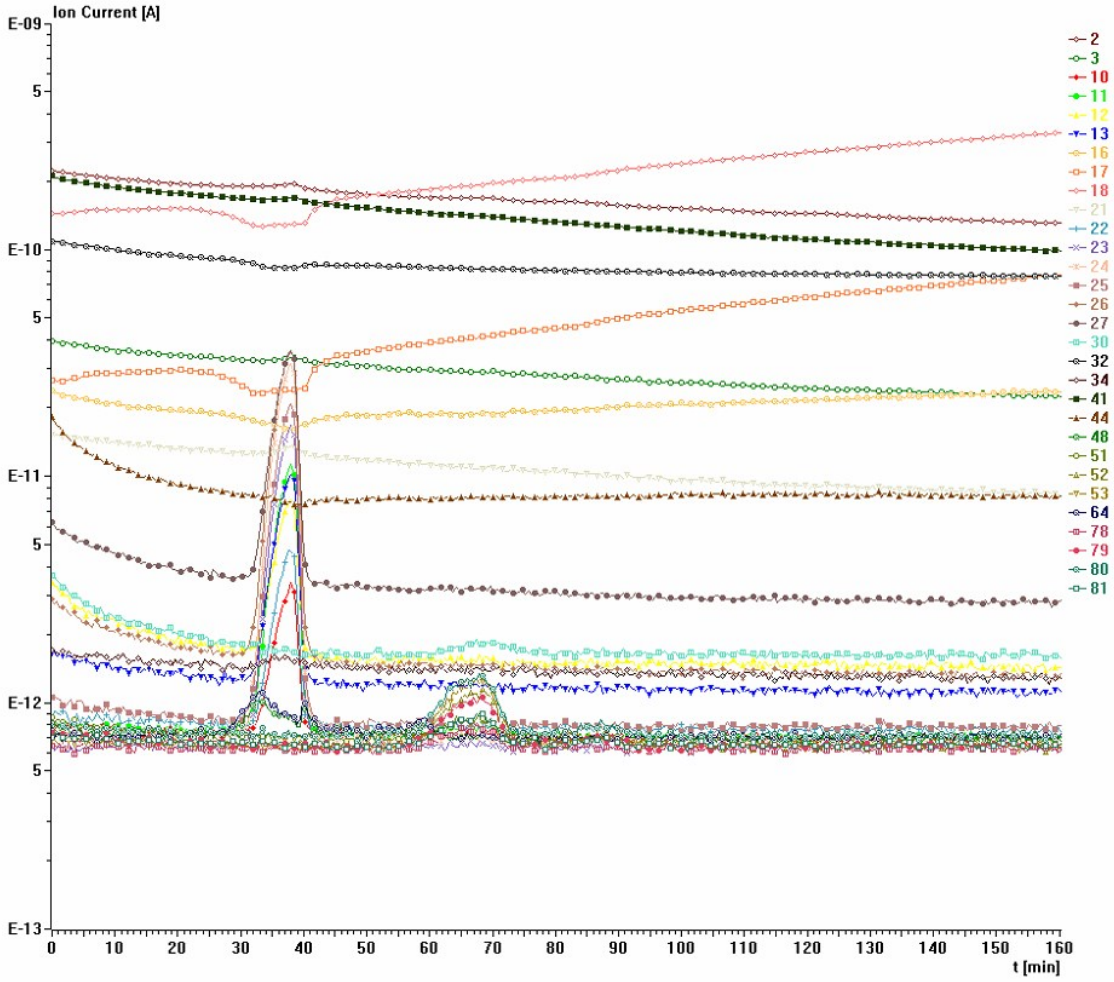

Figure S4. Mass spectra of gaseous decomposition products of compound **2**. Time range shown in the figure corresponds to temperature range -20-300 °C, heating rate 2 °C/min. Two main events can be observed at the time corresponding to the ranges of 40-65 °C and 95-125 °C.

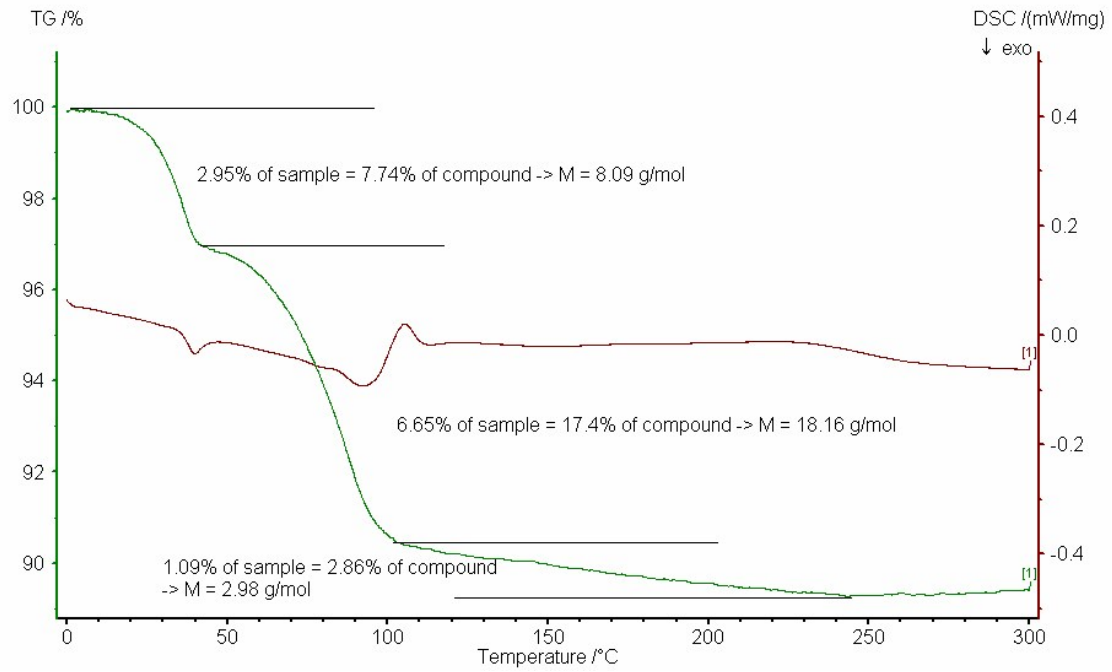

Figure S5. TGA/DSC plots of $NH_4[Al(BH_4)_4]$ (**3**) with quantitative details on mass drop events.

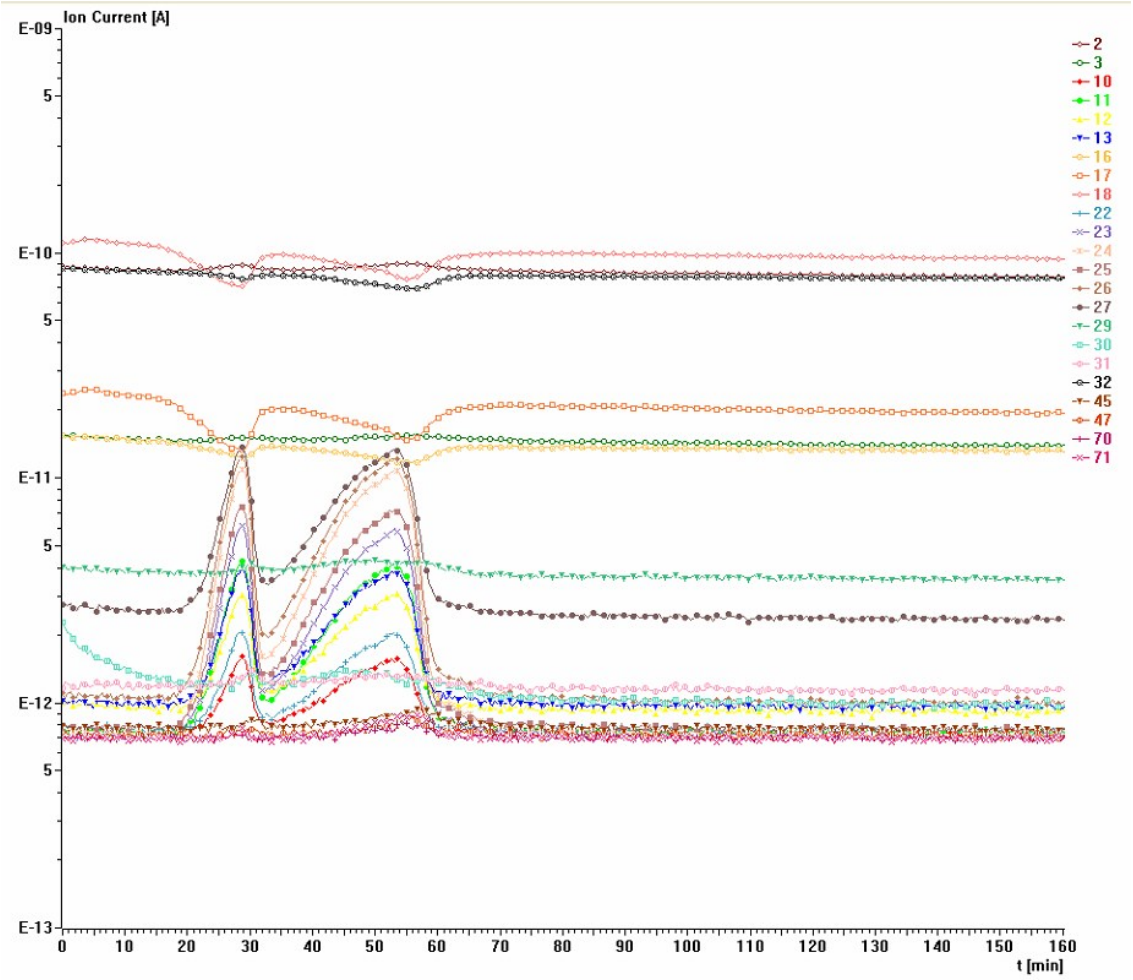

Figure S6. Mass spectra of gaseous decomposition products of compound **3**. Time range shown in the figure corresponds to temperature range -20–300 °C, heating rate 2 °C/min. Maxima of two main events can be observed at the time corresponding to 38 °C and 87 °C.

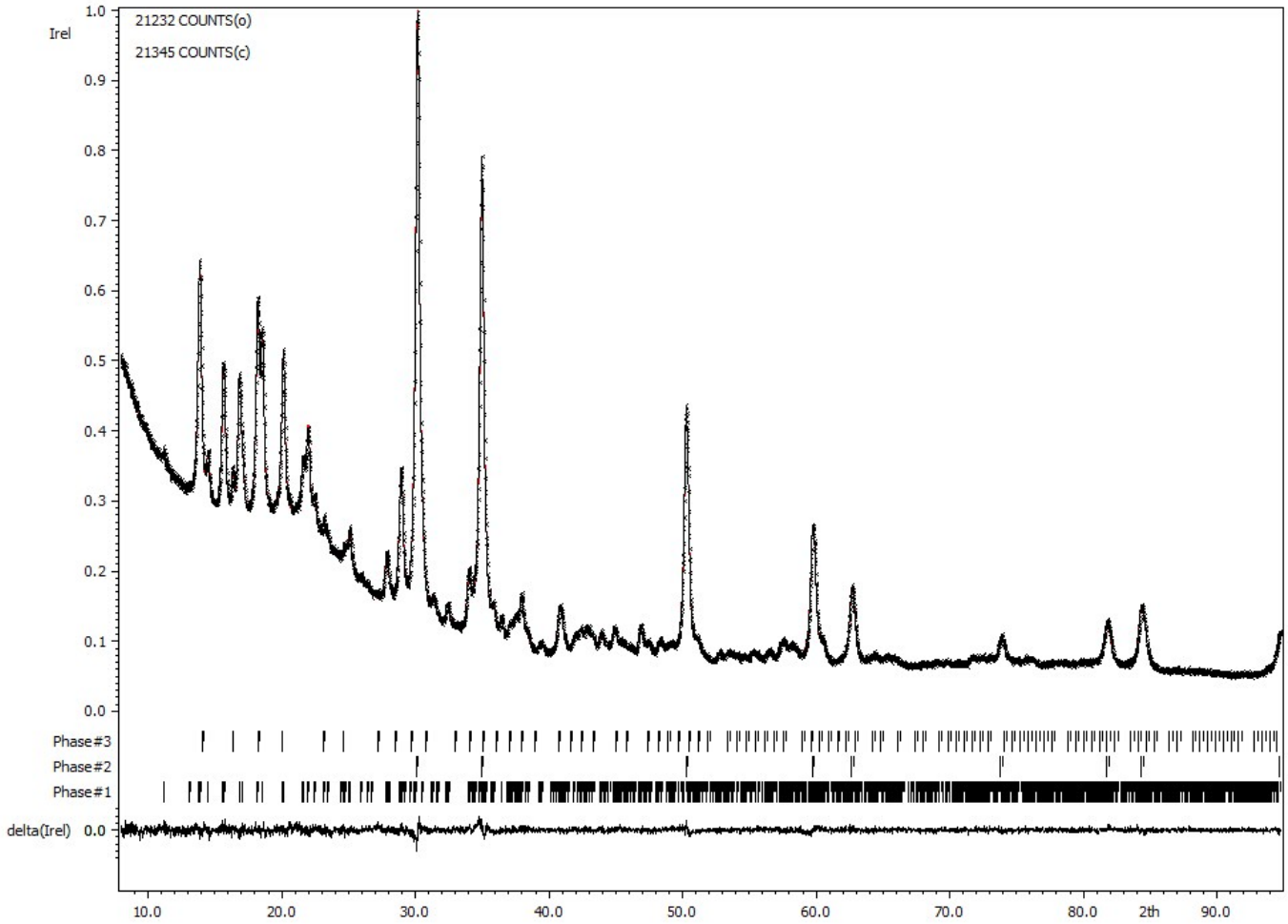

Figure S7. Rietveld plot of $NH_4[Y(BH_4)_4]$ at 233 K. Phase#1 - $NH_4[Y(BH_4)_4]$, Phase#2 - LiCl, Phase#3 - α-$Y(BH_4)_3$.

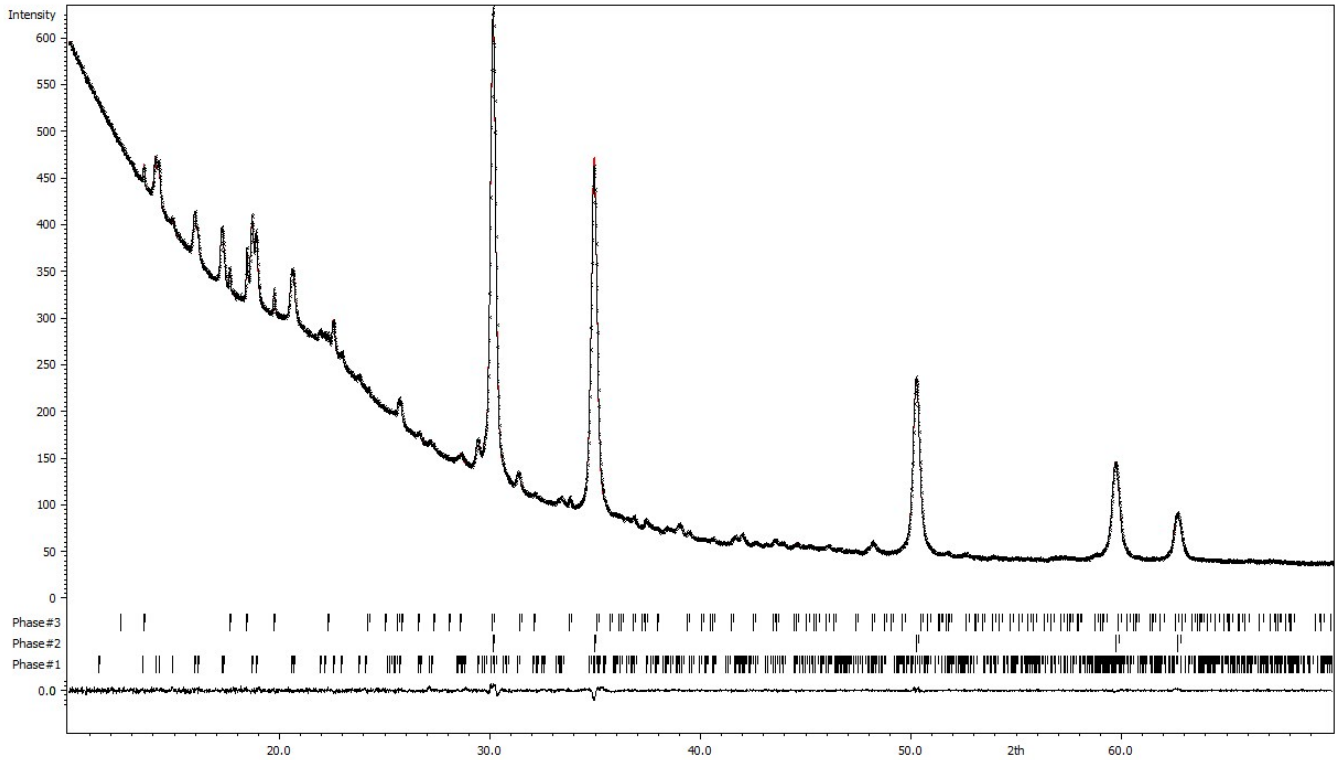

Figure S8. Rietveld plot of $NH_4[Sc(BH_4)_4]$ at 240 K. Phase#1 - $NH_4[Sc(BH_4)_4]$, Phase#2 - LiCl, Phase#3 - β-$Li[Sc(BH_4)_4]$.

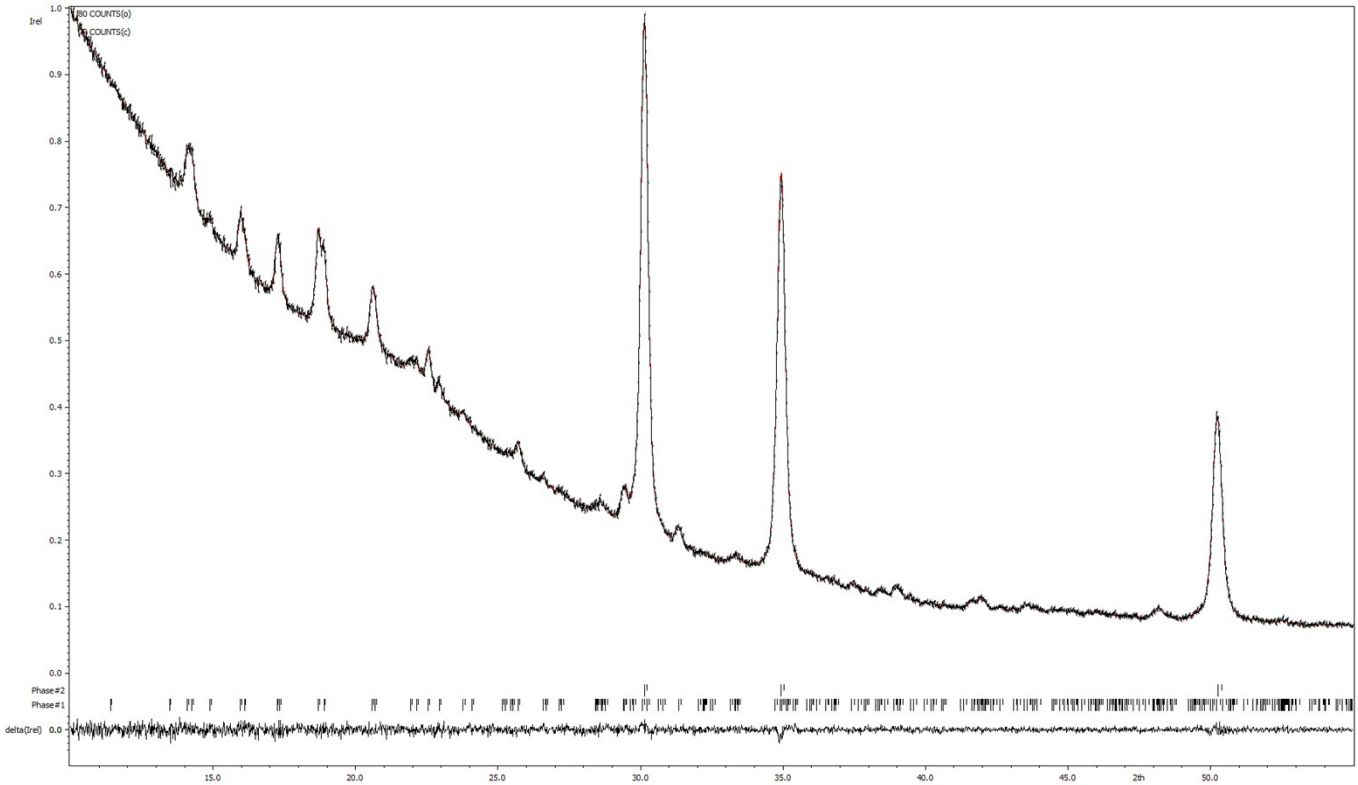

Figure S9. Rietveld plot of $NH_4[Sc(BH_4)_4]$ at 240 K. Phase#1 - $NH_4[Sc(BH_4)_4]$, Phase#2 - LiCl. This data is lower quality than the one from Figure S8, but shows sample without β-$Li[Sc(BH_4)_4]$.

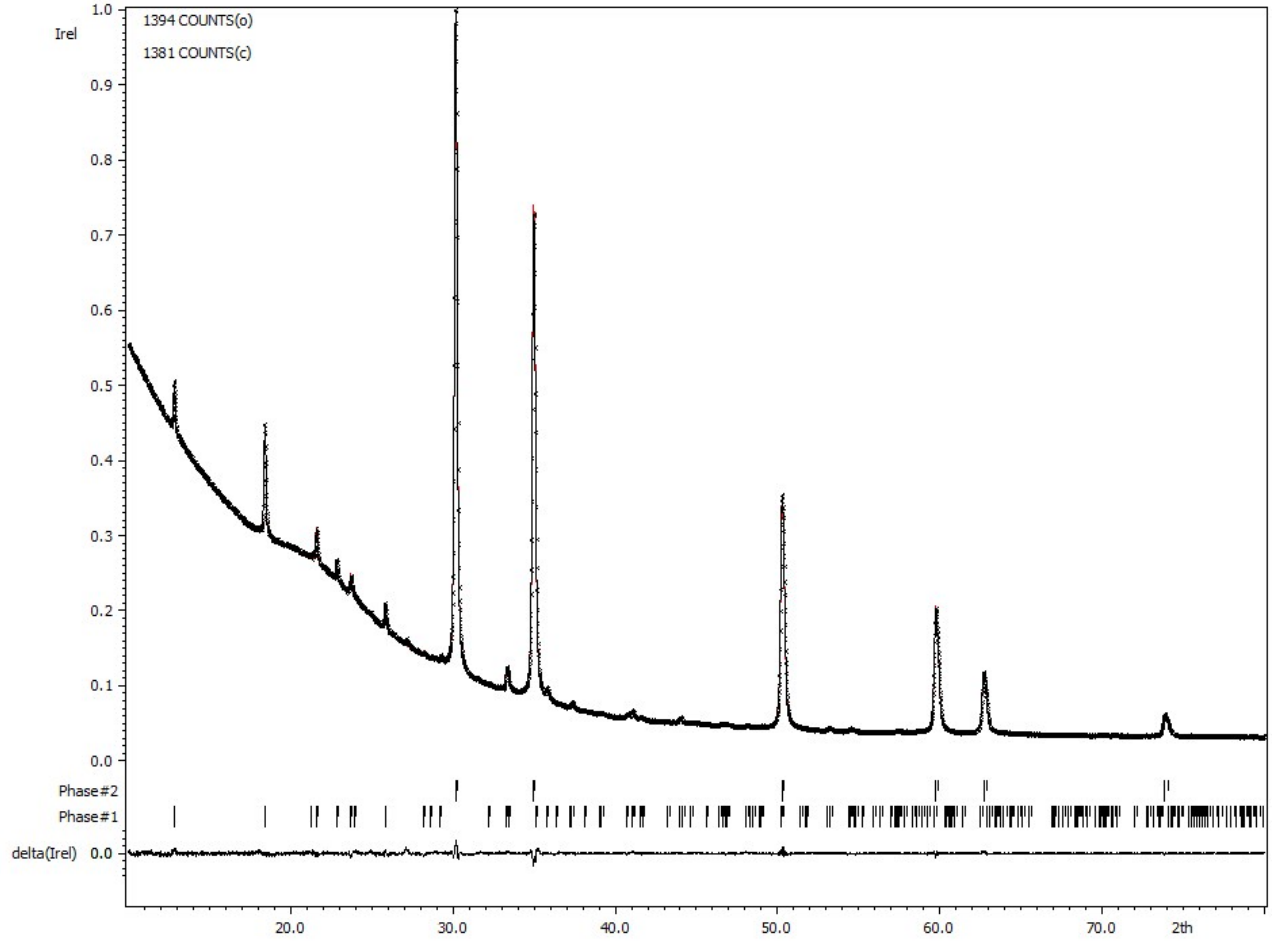

Figure S10. Rietveld plot of $NH_4[Al(BH_4)_4]$ at 240 K. Phase#1 - $NH_4[Al(BH_4)_4]$, Phase#2 - LiCl.

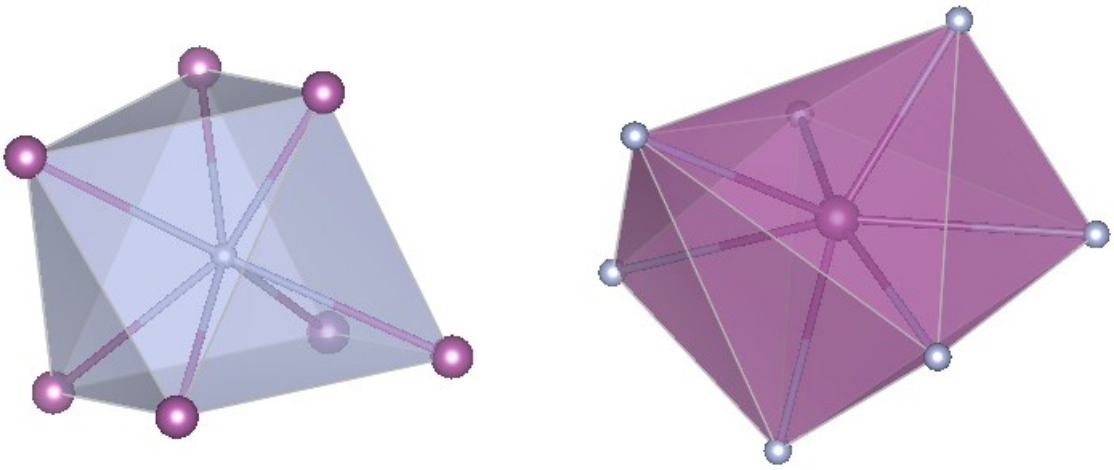

Figure S11. Anions-cations coordination polyhedra in compounds **1** and **2**. Since N atoms (gray) and Sc/Y atoms (purple) are central atoms of NH_4^+ cations and $[M(BH_4)_4]^-$ anions, respectively, H and B atoms are not shown in the picture for clarity.

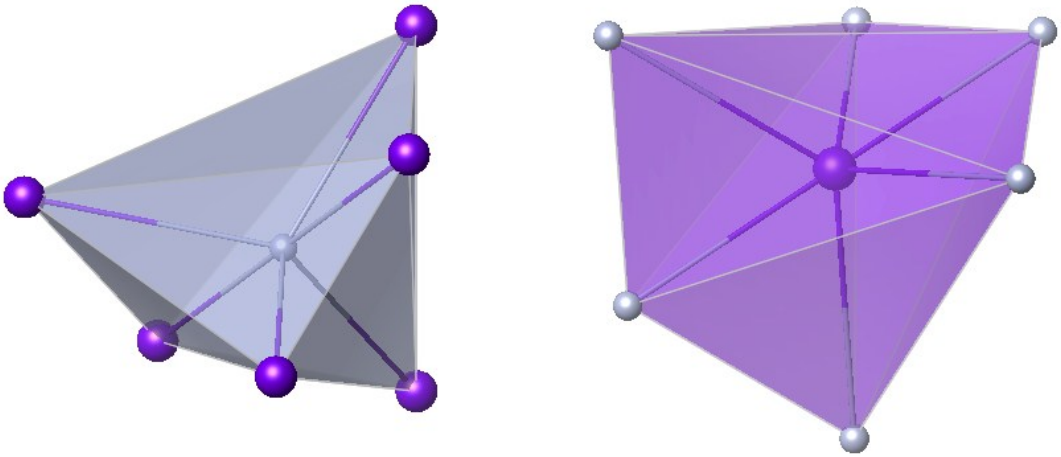

Figure S12. Anions-cations coordination polyhedra in compound **3**. Since N atoms (gray) and Al atoms (violet) are central atoms of NH_4^+ cations and $[Al(BH_4)_4]^-$ anions, respectively, H and B atoms are not shown in the picture for clarity.

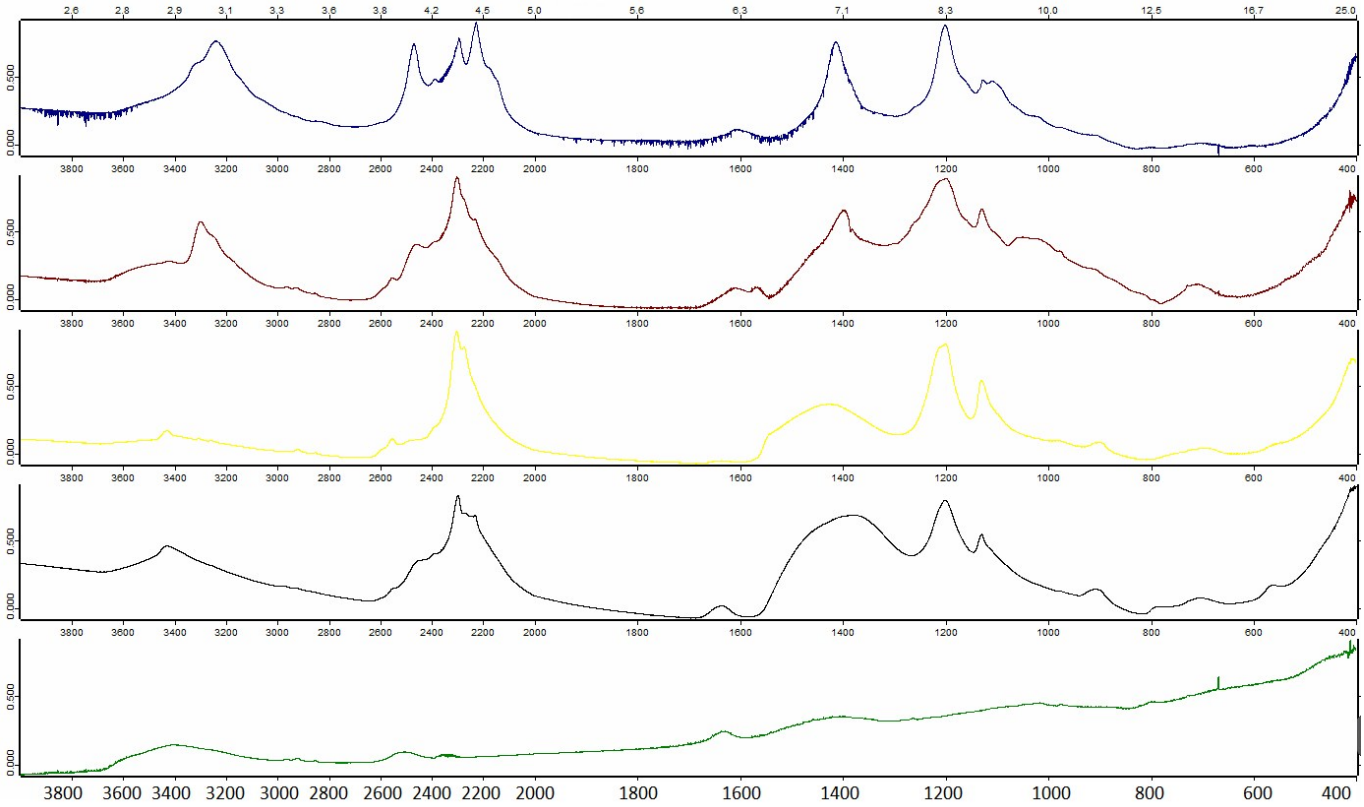

Figure S13. FTIR spectra of compound **1** heated up to different temperatures: 240 K, RT, 160 °C, 210 °C and 300 °C, starting from top.

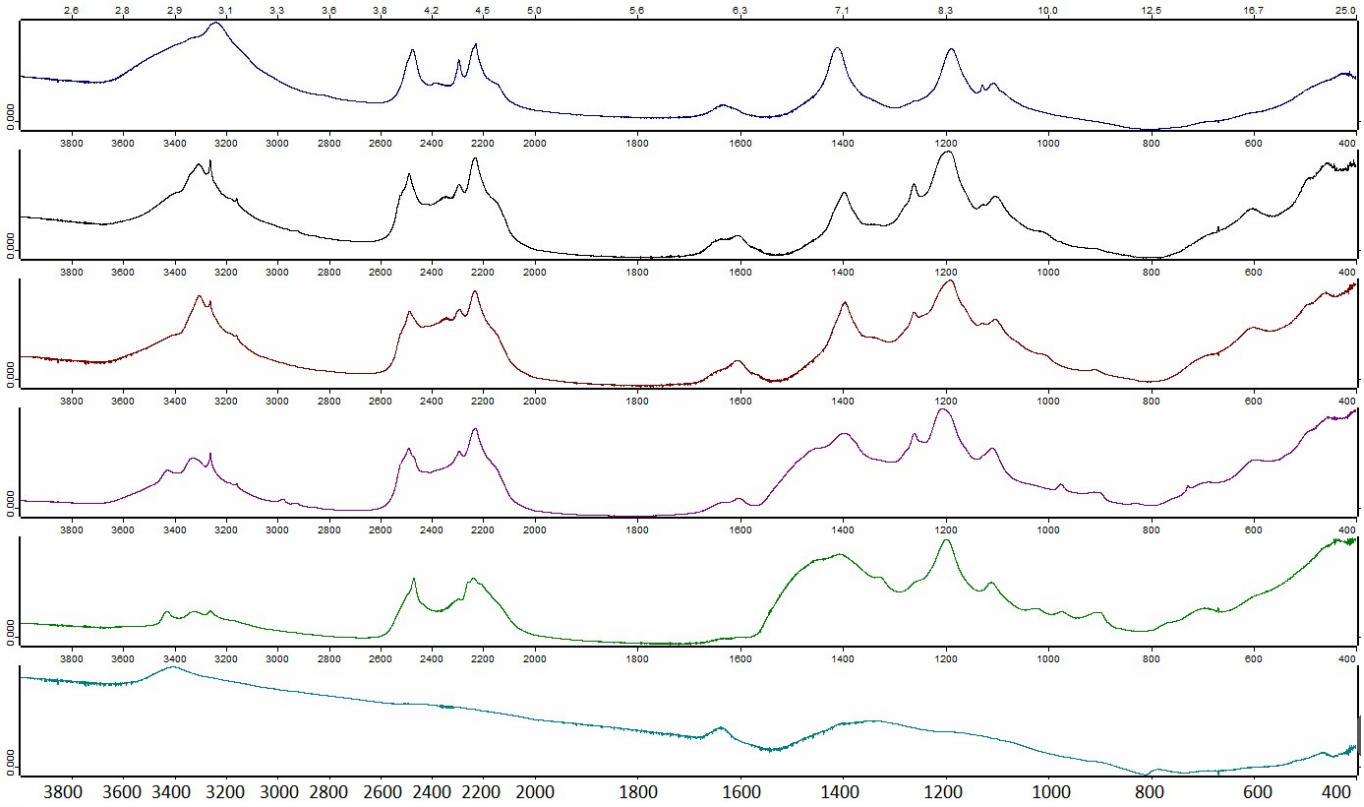

Figure S14. FTIR spectra of compound **2** heated up to different temperatures: 240 K, RT, 80 °C, 120 °C, 140 °C and 300 °C, starting from top.

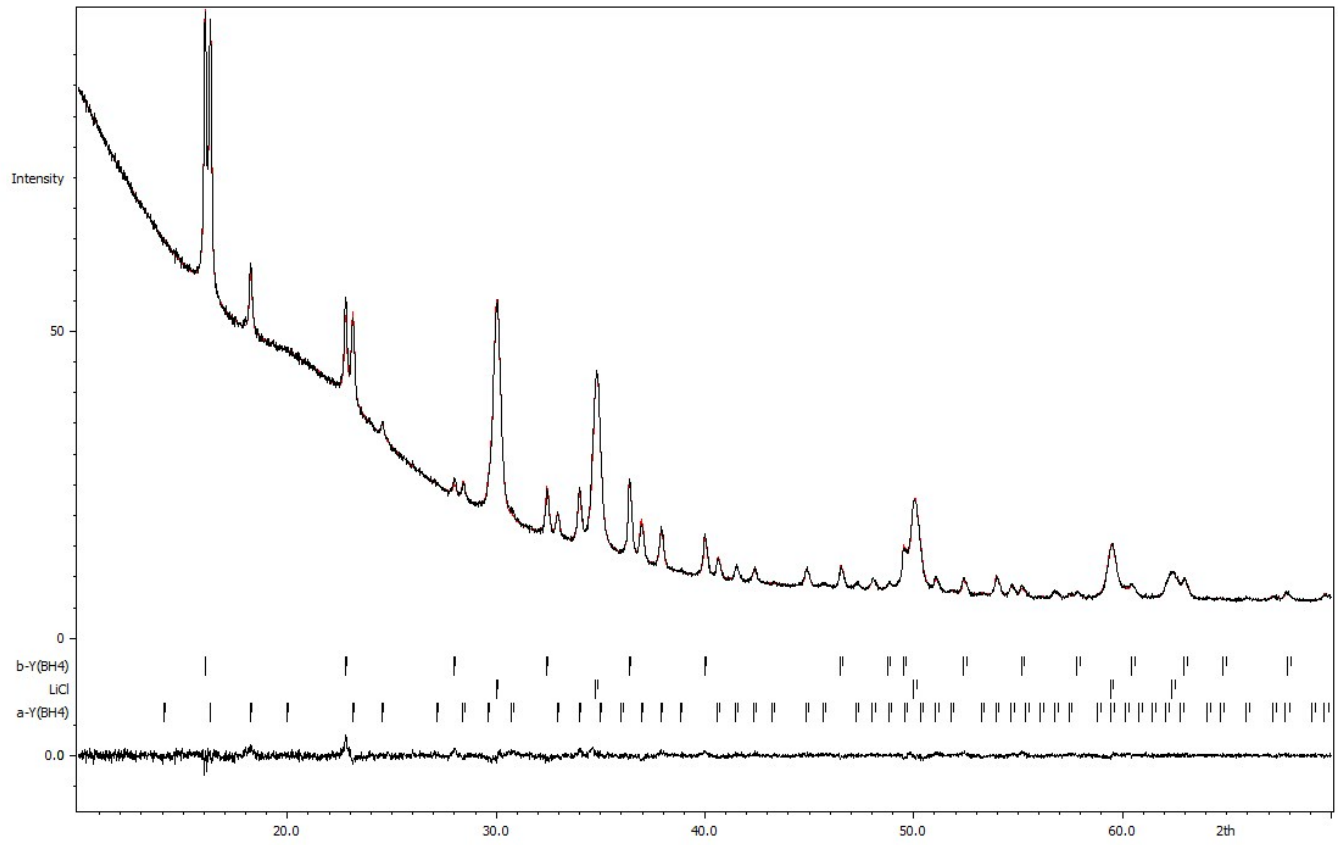

Figure S15. Rietveld plot of compound **1** at RT. Phases, starting from bottom, α-$Y(BH_4)_3$, LiCl and β-$Y(BH_4)_3$.

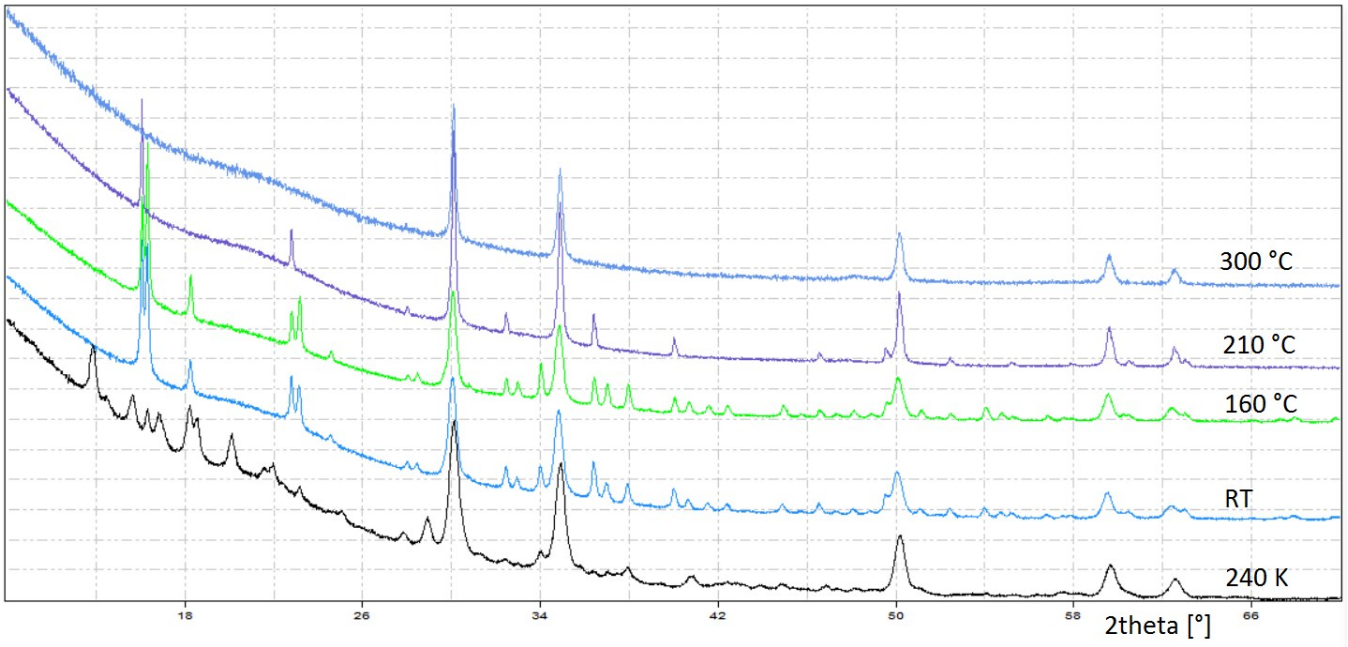

Figure S16. XRD patterns of compound **1** at different temperatures. Samples composition: 240 K - $NH_4[Y(BH_4)_4]$ and LiCl; RT - α-$Y(BH_4)_3$, β-$Y(BH_4)_3$ and LiCl; 160 °C - α-$Y(BH_4)_3$, β-$Y(BH_4)_3$ and LiCl; 210 °C - β-$Y(BH_4)_3$ and LiCl; 300 °C - LiCl.

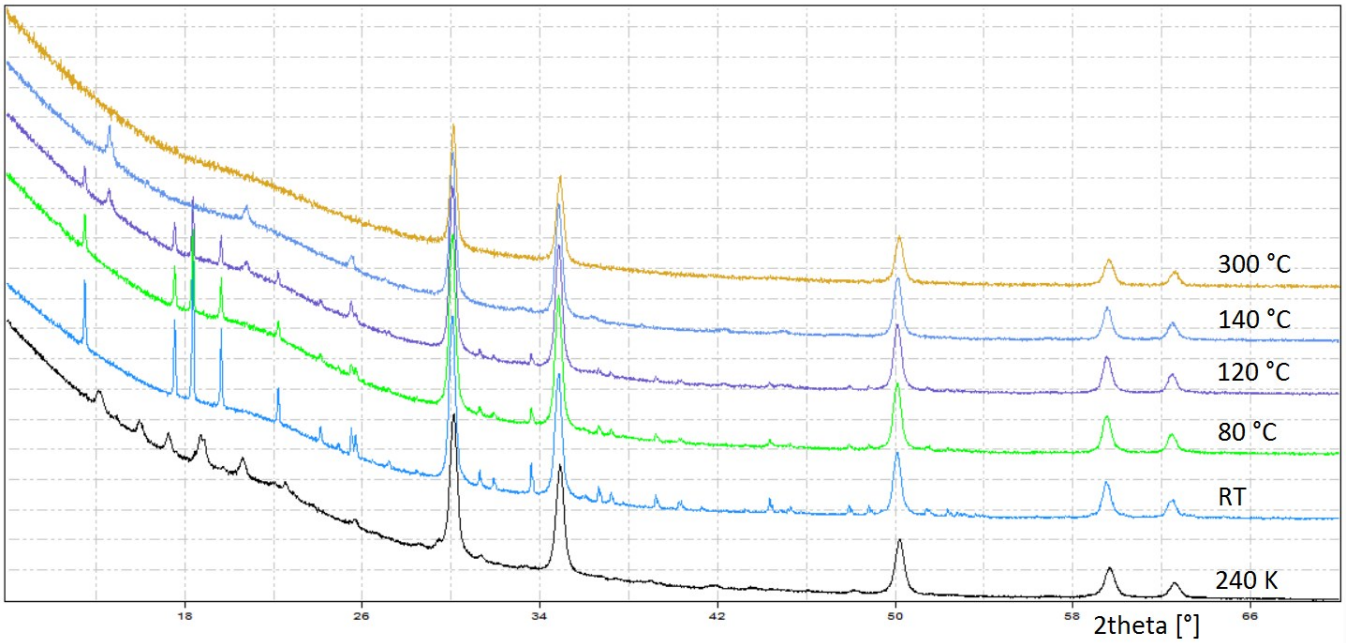

Figure S17. XRD patterns of compound **2** at different temperatures. Samples composition: 240 K - $NH_4[Sc(BH_4)_4]$ and LiCl; RT - β-$Li[Sc(BH_4)_4]$ and LiCl; 80 °C - β-$Li[Sc(BH_4)_4]$ and LiCl; 120 °C - β-$Li[Sc(BH_4)_4]$, α-$Li[Sc(BH_4)_4]$ and LiCl; 140 °C - α-$Li[Sc(BH_4)_4]$ and LiCl; 300 °C - LiCl.

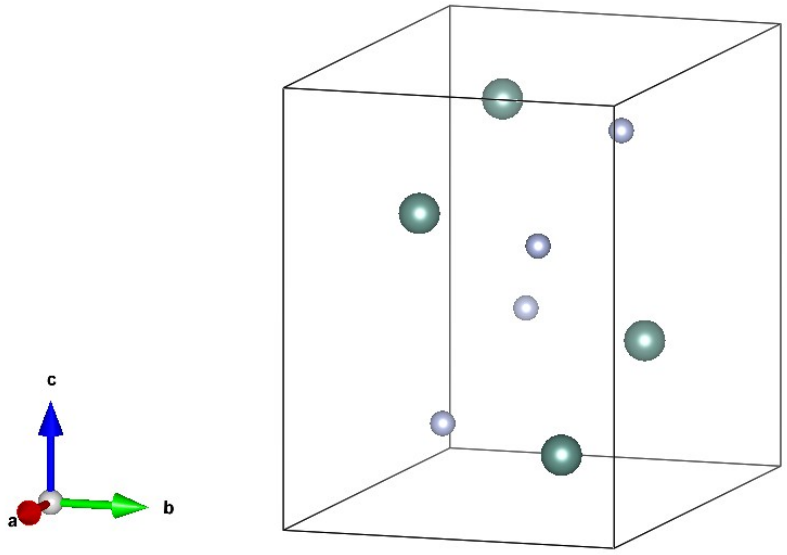

Figure S18. Crystal cell of Y/N (green and gray, respectively) sublattice in $NH_4[Y(BH_4)_4]$ (**1**): orthorhombic *P*nma, a = 12.202 Å, b = 8.076 Å, c = 10.378 Å.

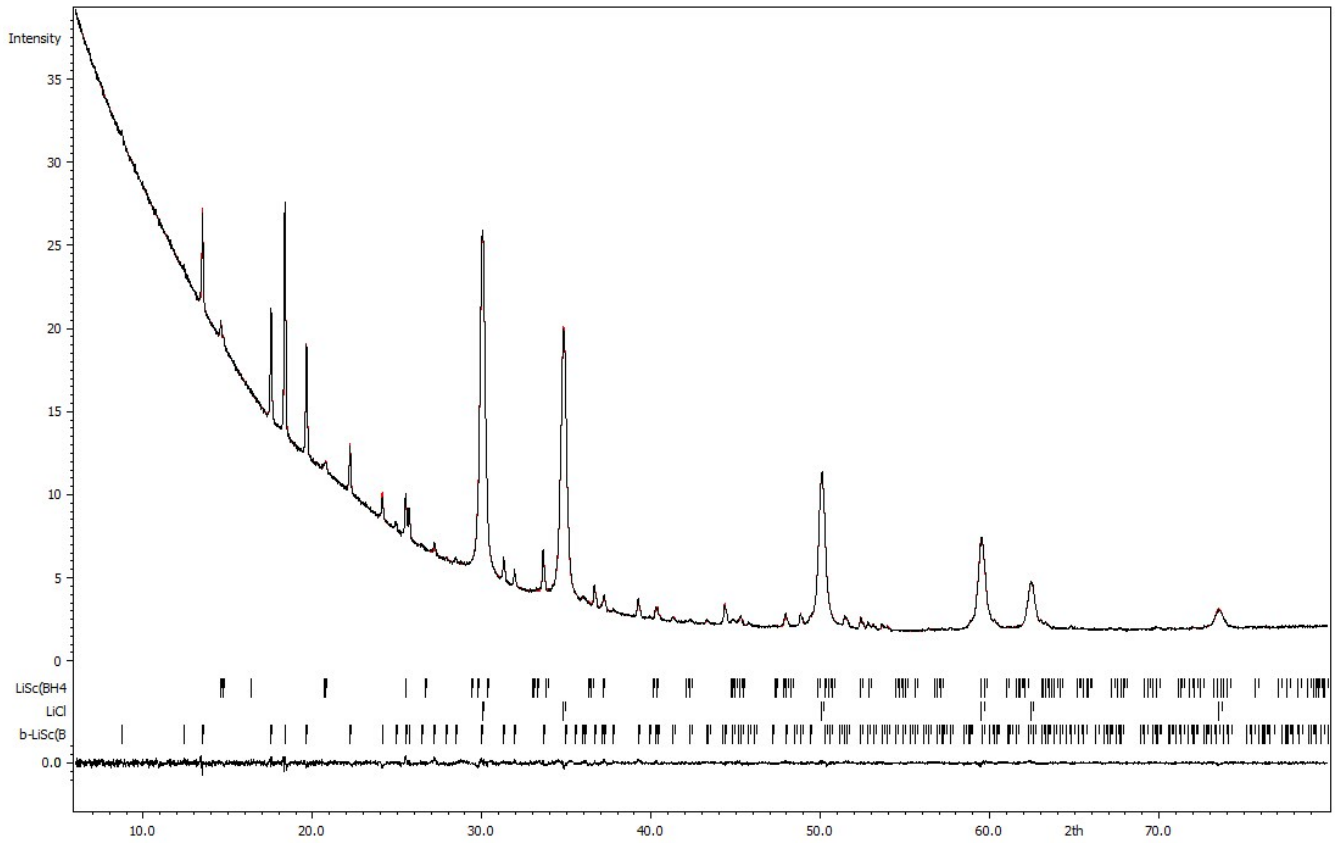

Figure S19. Rietveld plot of β-Li[Sc(BH_4)$_4$] at RT. Phases, from bottom to top, β-Li[Sc(BH_4)$_4$], LiCl, α-Li[Sc(BH_4)$_4$].

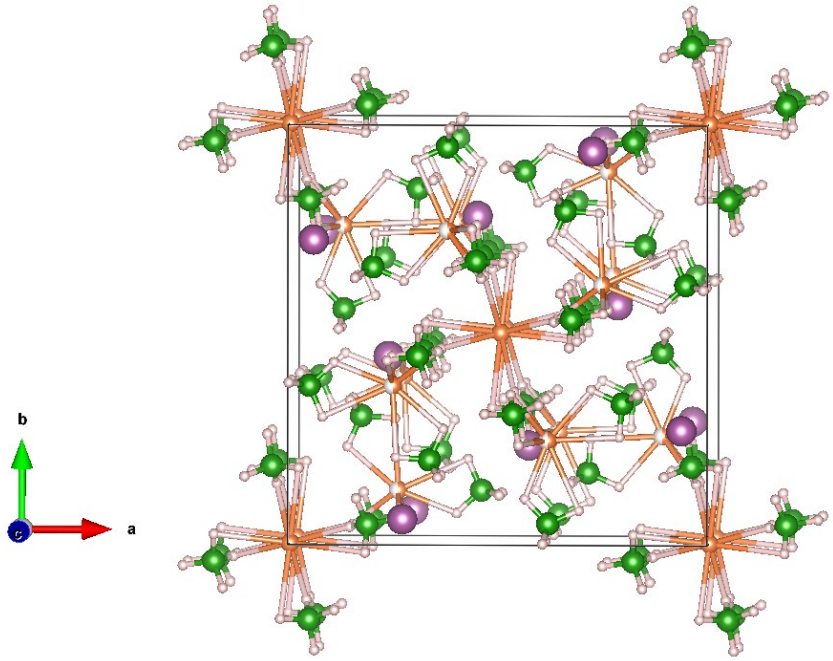

Figure S20. Li@H coordination in β-Li[Sc(BH_4)$_4$].

Table S1. Elemental combustion analysis results of compounds **1**, **2** and **3** at RT (shaded rows) with comparison to $NH_4[M(BH_4)_4]$ wt% composition and solid products of possible decomposition reaction routes.

Compound	Cl content [wt%]	N content [wt%]	H content [wt%]
$NH_4[Y(BH_4)_4]$ (**1**) + 4 LiCl	42.22	4.17	6.00
1 at RT + 4 LiCl	40.40-40.64	3.69-3.76	3.18-3.25
After reaction route: $NH_4[Y(BH_4)_4]$ + 4 LiCl ⟶ $Y(BH_4)_3$ + 4 H_2+ a-BN + 4 LiCl	43.26	4.27	3.69
$NH_4[Sc(BH_4)_4]$ + 4 LiCl	48.56	4.80	6.91
2 at RT + 4 LiCl	49.33-49.58	4.84-4.94	4.40-4.58
$NH_4[Sc(BH_4)_4]$ + 4 LiCl ⟶ $Sc(BH_4)_3$ + 4 H_2+ a-BN + 4 LiCl	49.96	4.93	4.26
$NH_4[Al(BH_4)_4]$ (**3**) + 4 LiCl	51.76	5.11	7.36
3 at RT + 4 LiCl	54.23	5.01-5.06	3.88-3.94
After reaction route: $NH_4[Al(BH_4)_4]$ + 4 LiCl ⟶ 4 H_2+ {$Al(BH_4)_3$ x BN} + 4 LiCl	53.33	5.27	4.55
After reaction route: $NH_4[Al(BH_4)_4]$ + 4 LiCl ⟶{$HAl(BH_4)_2$ x NH_2BH_2} + ½ B_2H_6 + 2H_2 + 4 LiCl	55.37	5.47	5.12
After reaction route: $NH_4[Al(BH_4)_4]$ + 4 LiCl ⟶{H_2AlBH_4 x NH_2BH_2} + B_2H_6 + H_2 + 4 LiCl	58.78	5.81	5.01

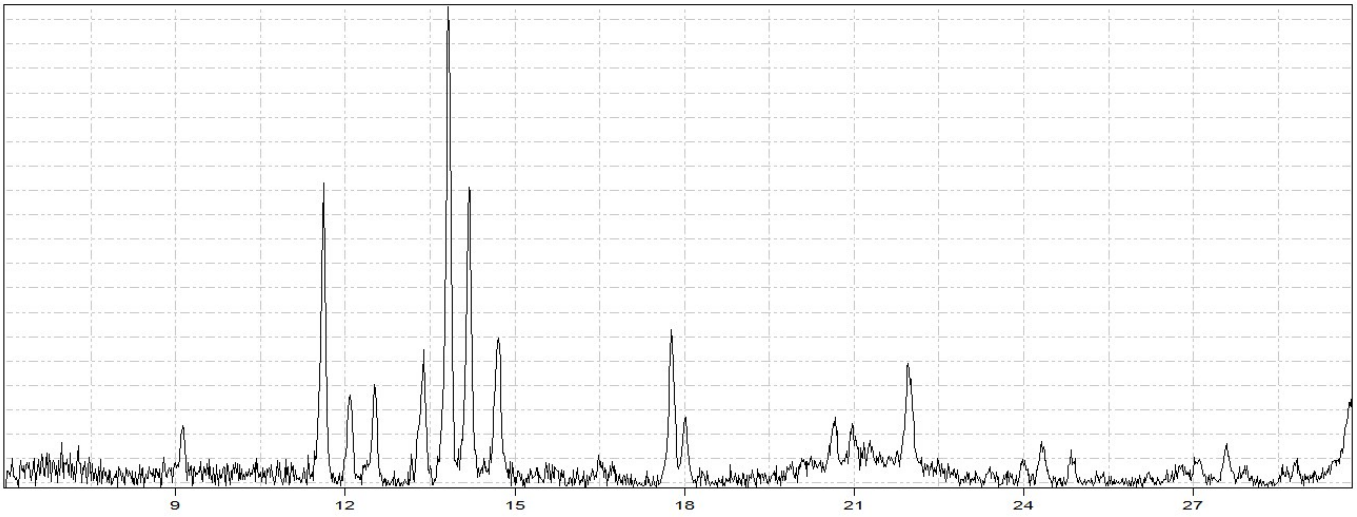

Figure S21. XRD pattern of the product of RT decomposition of the compound **3** (the low-angle part). The background has been removed for clarity. The diffraction peaks can be indexed in two monoclinic unit cells: $P2_1/c$-type, a = 8.7840 Å, b = 13.3137 Å, c = 16.2906 Å, beta = 119.9005°; $P2_1/n$-type, a = 14.1477 Å, b = 13.3227 Å, c = 8.7911 Å, beta = 92.7022°.